

Communication

Design of a Single-Sided, Coreless, Flat-Type Linear Voice Coil Motor

Wei Zhang, He Zhang ^{*}, Junren Mu and Song Wang

School of Electrical-Engineering and Automation, Harbin Institute of Technology, Harbin 150001, China

^{*} Correspondence: h.zhang@hit.edu.cn

Abstract: A voice coil motor is a type of permanent magnet linear motor, which is based on the Ampere force theorem. It has the following advantages: a simple structure, a small size, no cogging force, and a fast response time. In this study, a voice coil motor was designed to provide x-directional thrust in the magnetically levitated cable table of a lithography machine. The voice coil motor designed in this study was based on the Halbach permanent magnet array, and adopted a single-sided, coreless, flat-type structure. First, the magnetic field distribution was analyzed based on the magnetic charge method to obtain an expression for the magnetic field and the thrust. The results of this analysis agreed very well with the finite element simulation results. Next, the main parameters of the motor, including the number of turns made by the coil, the size of the wire, and the size of the permanent magnets, were selected and optimized to increase the force density. Finally, two double-layer, serpentine waterway water-cooling plate configurations were designed for this voice coil motor. The validity of this water-cooling structure was verified for two different winding equivalent models. This provided feasibility to further upgrade the windings' current density.

Keywords: voice coil motor; Halbach permanent magnet array; magnetic field analysis; water cooling design



Citation: Zhang, W.; Zhang, H.; Mu, J.; Wang, S. Design of a Single-Sided, Coreless, Flat-Type Linear Voice Coil Motor. *Actuators* **2023**, *12*, 77. <https://doi.org/10.3390/act12020077>

Academic Editor: Junhui Hu

Received: 20 December 2022

Revised: 1 February 2023

Accepted: 8 February 2023

Published: 11 February 2023



Copyright: © 2023 by the authors. Licensee MDPI, Basel, Switzerland. This article is an open access article distributed under the terms and conditions of the Creative Commons Attribution (CC BY) license (<https://creativecommons.org/licenses/by/4.0/>).

1. Introduction

Before linear motors were widely used, most linear motion had to be generated using mechanical structures, such as rotary motors and gears, which were clearly not the best way to generate linear motion due to the short life span and low efficiency of the mechanical structures. The linear motor does not require an intermediate transmission device and can directly convert electrical energy into mechanical energy for linear motion. Compared with the rotary motor drive, it has the following advantages: a simple system structure, high reliability, high precision, high efficiency, a fast response time, good flexibility, and a low cost. Consequently, in recent years, it has been widely used in transportation, machining, precision control, and other fields [1,2].

The voice coil motor is so-named because its shape is very similar to the acoustic coil used in loudspeakers. It is a special linear motor, which generates driving force through the interaction of a magnetic field and an energized coil [3]. It has the following advantages: a simple structure, a fast dynamic response time, no cogging force, high linearity, etc. The linear servo system is directly driven by voice coil motors, and can effectively solve some of the shortcomings of using a traditional rotary motor with a ball-screw drive, through its high dynamic performance and high positioning accuracy [4]. With the development of design and control technology, the application field of voice coil linear motors has been further expanded, and they are widely used in a variety of closed-loop drive, short-range servo systems [5]. Compared to conventional linear motors, voice coil motors tend to have better high-frequency response characteristics, and are particularly suitable for high-speed reciprocating linear motion in short-stroke servo control systems because of their high positional accuracy [6].

In the field of automated equipment manufacturing, the movement of equipment is often disturbed by the cables. Generally, to solve this problem a special table that pulls the cable is necessary to track the position of the moving platform [7]. To this end, this paper has proposed the design of a 110N single-sided, flat-type voice coil motor to provide short-stroke lateral restraint in magnetically levitated cable tables.

The innovation of this study is mainly reflected in the following two aspects: (1) Its innovative application—voice coil motors are becoming more widely used, but combined applications in cable tables are rare, as application scenarios require high-precision and quick response times. (2) The design of a water-cooled plate—for small motors, the use of a double-layer, water-cooled plate structure is relatively rare, because of the small size of the motor and the high current density; therefore, a double-layer, water-cooled structure was adopted in this study.

2. Basic Structure and Analysis of the Voice Coil Motor's Operating Performance

2.1. Basic Structure and Working Principle

The motor that was designed in this study provides x-direction force, and can be used in combination with other motors in cable tables. The schematic diagram is shown in Figure 1. The coil of a voice coil motor is located in the air-gap magnetic field. Under an applied voltage, an electric current is generated in the coil and, according to the Ampere force principle, the energized wire will generate an electromagnetic force in the magnetic field. This electromagnetic force is proportional to the current; therefore, the motor movement can be precisely controlled by adjusting the current value. In this study, to achieve the magnetic levitation goal, we increased the force density of our motors and reduced the weight of the system, the Halbach array, which has a unilateral magnetic field enhancement effect, was used in conjunction with a coreless structure.

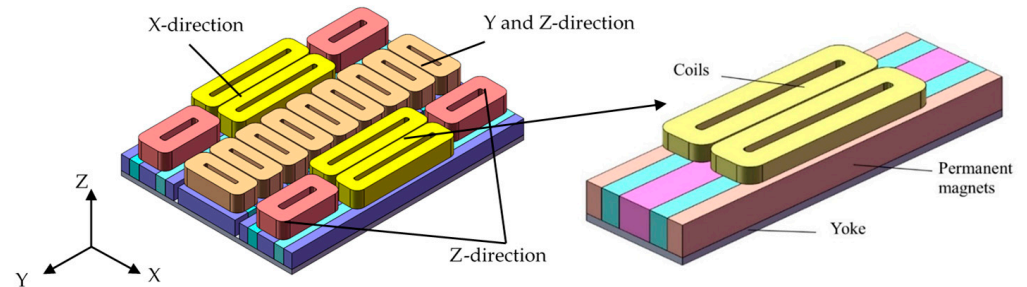


Figure 1. Schematic diagram of single-sided, coreless, flat-type linear voice coil motor.

2.2. Space Magnetic Field Analysis

In this paper, the magnetic field was analyzed by using the equivalent charge method, which assumes a body charge distribution inside the magnetized magnet, and a surface charge distribution at the magnet boundary.

The expression for the magnetic charge density of permanent magnets is as follows:

$$\rho_m = -\mu_0 \nabla \cdot \vec{M} \quad (1)$$

where μ_0 is vacuum permeability and \vec{M} is magnetization strength.

The expression for the magnetic charge density above the boundary of the permanent magnets is as follows:

$$\sigma_m = \mu_0 \vec{n} \cdot \vec{M} \quad (2)$$

where \vec{n} is the external normal unit vector.

Inside a permanent magnet with uniform parallel magnetization, the magnetization strength is constant and, therefore, $\rho_m = 0$. The equivalent surface magnetic charge of two sections along the magnetization direction can be used instead of the magnetic field

generated by the permanent magnet. The overall distribution of the magnetic field in space can be obtained by calculating the distribution of the magnetic field generated by one charge surface in the air. The residual magnetization strength of a permanent magnet can be used to express the equivalent magnetic charge surface density along the magnetization direction for uniform parallel magnetization, as follows:

$$\sigma_m = \mu_0 M_r = B_r \tag{3}$$

$$dQ_m = \sigma_m ds \tag{4}$$

$$d\vec{H} = \frac{dQ_m}{4\pi r^2} \vec{a}_r \tag{5}$$

where B_r is the residual magnetic density of permanent magnets; ds is the area of any micro-element taken on the magnetic charge plane; dQ_m is the amount of magnetic charge contained in a micro-element of area; r is the distance from the origin to the field point; \vec{a}_r is the unit vector from the origin to the field point; and $d\vec{H}$ is the magnetic field strength.

The following is the derivation of the expression for the magnetic field of a vertically magnetized permanent magnet, using permanent magnet III, shown in Figure 2, as an example. The decomposition of the spatial magnetic field of vertically magnetized and horizontally magnetized permanent magnets is shown in Figure 3.

$$dH_z = d\vec{H} \cdot \cos\theta = d\vec{H} \cdot \frac{z}{\sqrt{(x-x_0)^2 + (y-y_0)^2 + z^2}} \tag{6}$$

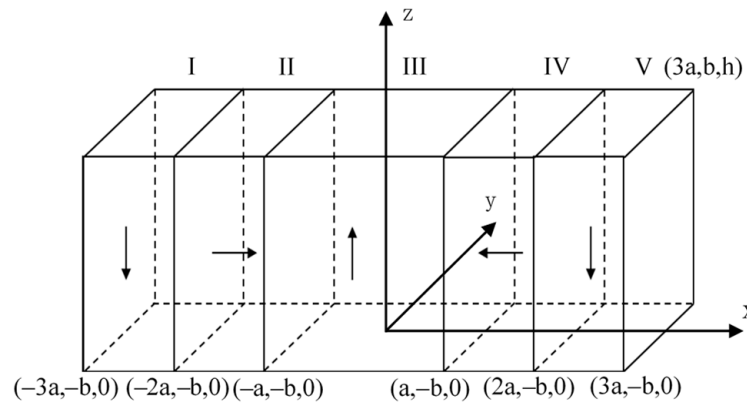


Figure 2. Schematic diagram of the Halbach permanent magnet array.

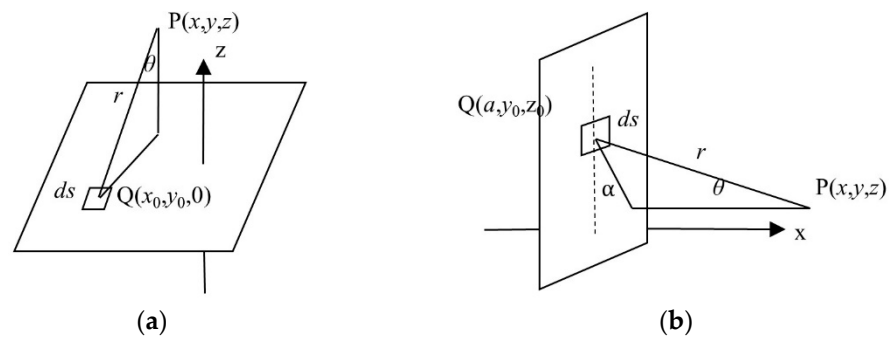


Figure 3. Schematic diagram of the vertical (a) and horizontal (b) magnetic charge surface that generates the space magnetic field.

The auxiliary function was introduced as follows:

$$\zeta(\zeta_1, \zeta_2, \zeta_3) = \operatorname{arctg} \frac{\zeta_1 \cdot \zeta_2}{\zeta_3 \cdot \sqrt{\zeta_1^2 + \zeta_2^2 + \zeta_3^2}} \quad (7)$$

$$K = \frac{\mu_0 M_r}{4\pi} \quad (8)$$

The expression for the z-axis component of the spatial flux density produced by permanent magnet III ($2a \times 2b \times h$) was obtained, as follows:

$$\begin{aligned} B_{IIIz} = & K[\zeta(x-a, y-b, z-h) - \zeta(x-a, y+b, z-h) \\ & - \zeta(a+x, y-b, z-h) + \zeta(a+x, y+b, z-h) \\ & - \zeta(x-a, y-b, z) + \zeta(x+a, y+b, z) \\ & + \zeta(x+a, y-b, z) - \zeta(a+x, y+b, z)] \end{aligned} \quad (9)$$

Using permanent magnet IV as an example, we derived an expression for the spatial magnetic field of a horizontally magnetized permanent magnet, as follows:

$$dH_x = \vec{dH} \cdot \cos \theta = d\vec{H} \cdot \frac{x-a}{\sqrt{(x-a)^2 + (y-y_0)^2 + (z-z_0)^2}} \quad (10)$$

$$dH_z = \vec{dH} \cdot \sin \theta \cdot \cos \alpha = d\vec{H} \cdot \frac{z-z_0}{\sqrt{(x-a)^2 + (y-y_0)^2 + (z-z_0)^2}} \quad (11)$$

The auxiliary function was introduced, as follows:

$$\delta(\delta_1, \delta_2, \delta_3) = \arcsin \frac{\delta_1 \cdot \delta_2}{\sqrt{\delta_3^2 + \delta_1^2} \cdot \sqrt{\delta_3^2 + \delta_2^2}} \quad (12)$$

$$\gamma(\gamma_1, \gamma_2, \gamma_3) = \ln(\gamma_2 + \sqrt{\gamma_1^2 + \gamma_2^2 + \gamma_3^2}) \quad (13)$$

The components of permanent magnet IV in the x-direction and z-direction of the spatial magnetic field were obtained as follows:

$$\begin{aligned} B_{IVx} = & K[-\delta(x-a, y-b, z-h) + \delta(x-a, y-b, z) \\ & + \delta(x-a, y+b, z-h) - \delta(x-a, y+b, z) \\ & + \delta(x-2a, y-b, z-h) - \delta(x-2a, y-b, z) \\ & - \delta(x-2a, y+b, z-h) + \delta(x-2a, y+b, z)] \end{aligned} \quad (14)$$

$$\begin{aligned} B_{IVz} = & K[-\gamma(x-a, y-b, z-h) + \gamma(x-a, y-b, z) \\ & + \gamma(x-a, y+b, z-h) - \gamma(x-a, y+b, z) \\ & + \gamma(x-2a, y-b, z-h) - \gamma(x-2a, y-b, z) \\ & - \gamma(x-2a, y+b, z-h) + \gamma(x-2a, y+b, z)] \end{aligned} \quad (15)$$

The analytical expression for the magnetic field generated by the permanent magnet was transformed by the coordinates, then the z-axis component of the magnetic flux density was superimposed using the following expression:

$$B_z = B_{Iz} + B_{IIz} + B_{IIIz} + B_{IVz} + B_{Vz} \quad (16)$$

2.3. Electromagnetic Force Analysis

For the voice coil motor designed in this study, since the main electromagnetic force was generated in the x-direction, only the electromagnetic force generated by the z-axis component of the spatial magnetic field acting in the coil was analyzed. If the end effects were not taken into account, the y-axis component of the spatial magnetic field was constant, and a micro-element, $dx \times dz$, was selected in the slot cross-section, and the expression for the electromagnetic force on the selected wire in the magnetic field was as follows:

$$dF_x = \bar{B}_z J_c dx dz l_{em} \quad (17)$$

where l_{em} is the effective length of the coil and \bar{B}_z is the average value of the z-axis component of the magnetic density within a micro-element.

The analytical results of the overall forces on the coils were obtained by iterative superposition of the selected sections.

3. Finite Element Simulation of Electromagnetic Fields

3.1. Parametric Modelling and Electromagnetic Performance Optimization

The aim of the dimensional parameters optimization of the permanent magnets and coils was to generate the maximum electromagnetic force. This was generated while the overall height of the motor and the overall width of the permanent magnets were kept constant.

The permanent magnet selected was the Arnold Nd-Fe-B N35. The remanent of this material was 1.21 T and the coercivity was 896 kA/m. The B-H curve was provided by the finite element software, JMAG. The main dimensional parameters in the motor cross-section are shown in Figure 4. As shown in Figure 5a, the motor generated the maximum electromagnetic force when the widths of permanent magnets I and II were almost equal. When the volume of the permanent magnets was increased, the air gap magnetic density was enhanced, whereas the coil space was compressed and the electromagnetic force was decreased, as shown in Figure 5b.

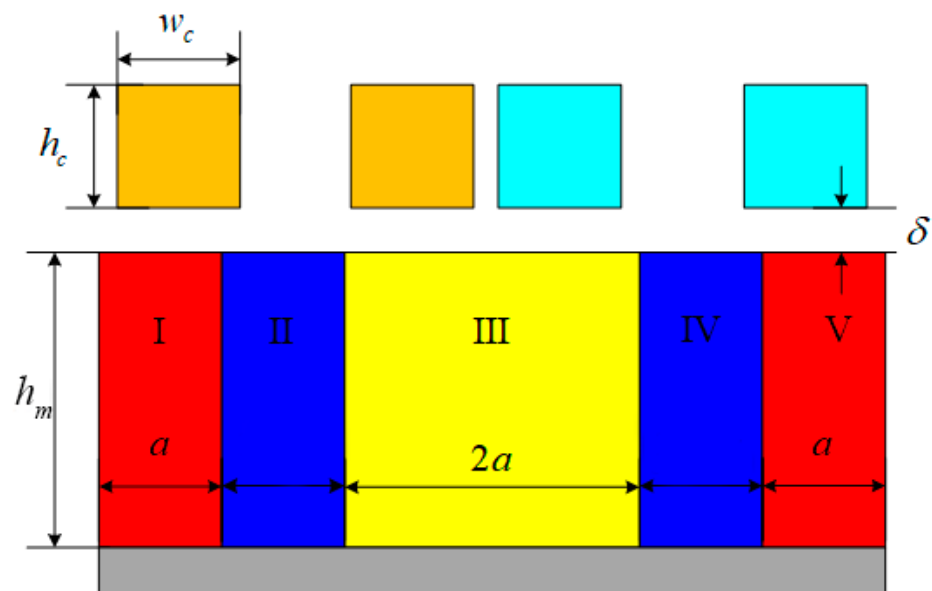


Figure 4. The main dimensional parameters in the motor's cross-section.

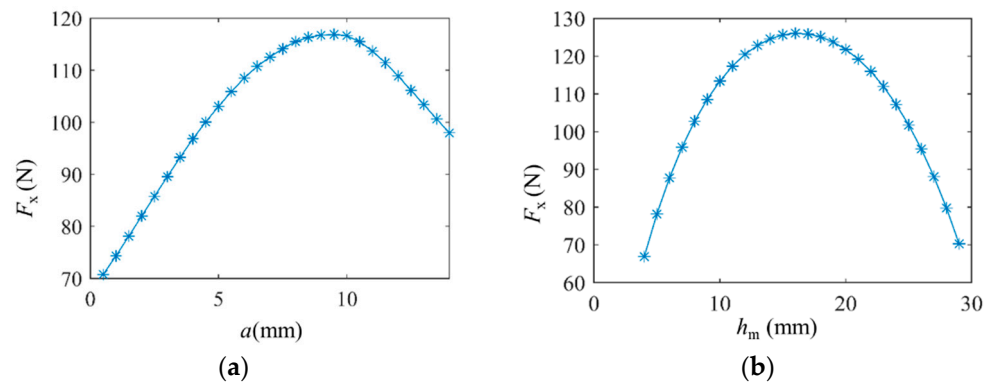


Figure 5. Relationship between electromagnetic force and permanent magnet width (a), and height (b) at $J = 13.33\text{A}/\text{mm}^2$.

3.2. Electromagnetic Performance Simulation

With reference to the results of each dimensional optimization, the main parameters of the voice coil motor are listed in the Table 1.

Table 1. Main parameters of the linear voice coil motor.

Variable Name	Value	Unit
Permanent magnet I width (a)	9.5	mm
Permanent magnet I height (h_m)	16	mm
Yoke width	60	mm
Yoke height	5	mm
Air gap length (δ)	3.4	mm
Number of turns of one coil	360	-
Effective coil length	99	mm
Coil cross-sectional area ($w_c \times h_c$)	12×18	mm^2
Cross-sectional area of single conductor	0.3×1.25	mm^2

As shown in Figure 6, we created twelve auxiliary lines in the space above the permanent magnet, six parallel to the x-axis, and another six parallel to the y-axis. Figure 7 shows our observations regarding the z-axis' magnetic flux density on the 12 auxiliary lines. Here, it can be seen that the analytical expressions for the magnetic field, which were obtained using the magnetic charge method, were correct and only differed minimally from the results of the finite element simulations. Furthermore, with the Halbach array, the iron yoke facilitated the enhancement of the air gap magnetic field; however, the effect was small.

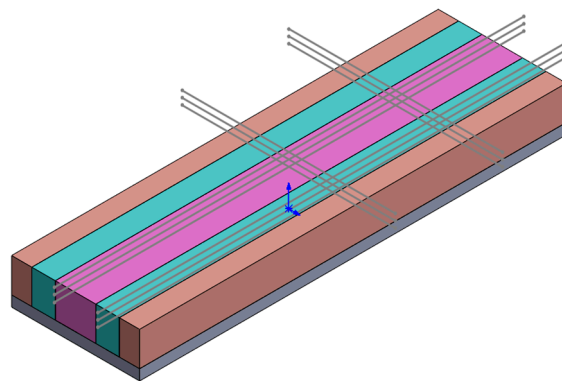


Figure 6. Schematic diagram of the test line location.

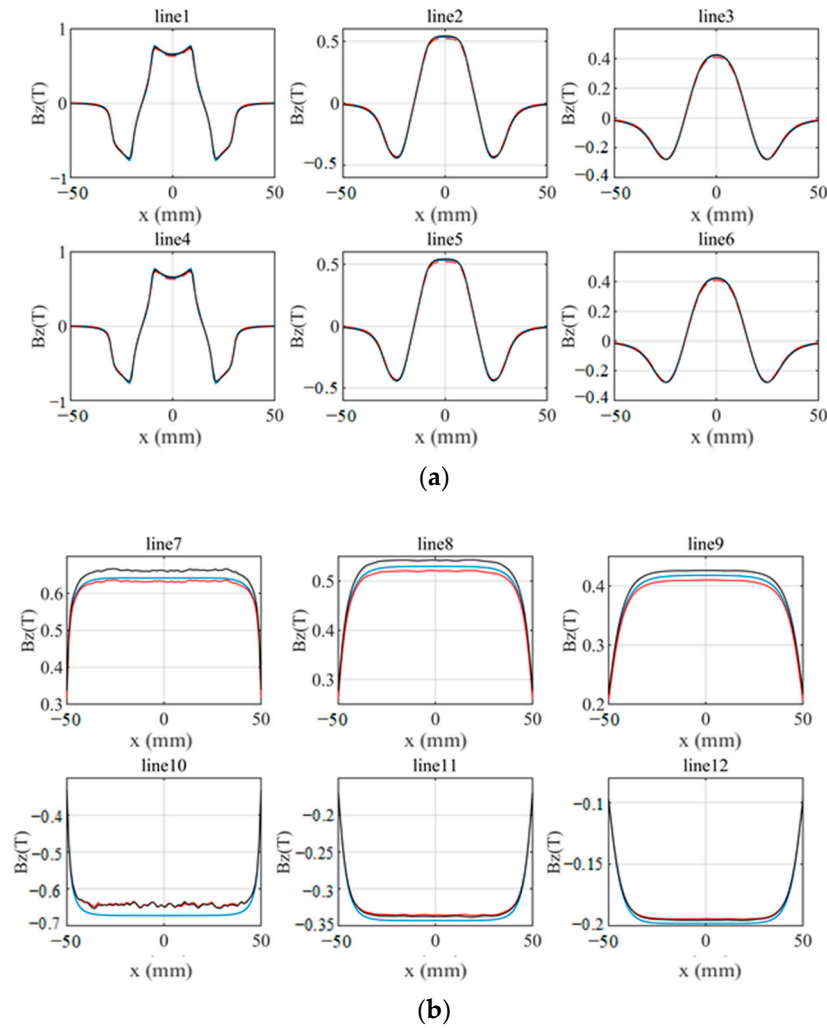


Figure 7. Permanent magnets' charge model verification (red—permanent magnet array, 3D simulation; blue—analytical solution; black—magnet array with 3D yoke simulation). (a) x-direction and (b) y-direction.

With a current density of 13.33 A/mm², the variation of the electromagnetic force on the coil at different coil displacements was obtained by means of analytical calculations and finite element simulations, respectively, as shown in Figure 8. The difference between the finite element simulation results and analytical results was less than 1%.

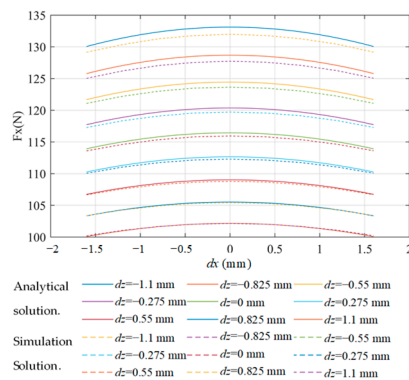


Figure 8. The relationship between the horizontal force of the coil and the displacement of the coil.

4. Water Cooling Structure Design and Temperature Rise Analysis

High temperature rises in voice coil motors can have an impact on their reliability, and the constant high temperature conditions can cause changes—even demagnetization—in the magnetic properties of permanent magnets. In this study, the small size and high current density of the voice coil motor that we designed made it extremely important to analyze its temperature field.

4.1. Cooling Structure Design

Two types of cooling structures are currently widely used for linear motors: the immersion type, and the water-jacketed construction [8]. The water-jacketed construction involves covering the windings with a cooling plate that has a cooling medium flow channel. Through this, the heat generated by the windings is transferred to the cooling medium, then the heat is transferred to the outside. The cooling effect of the water-jacket cooling method is lower than that of the immersion type because it has to undergo another heat transfer; however, the design process is relatively simple to implement and is not constrained by the material of the conductor. In this study, the cooling structure of the upper and lower water-cooled plates was adopted. Each cooling plate consisted of two layers of water channel plates, which were connected using structural adhesive. A cooling channel was formed inside by using upper and lower water channel plates.

Due to the small coil spacing, a set of water-cooled plates was used for the two coils. To increase the heat transfer area and to provide better cooling, we used a serpentine path for the waterway. When one inlet and one outlet waterway is used for cooling, the front end of the cooling waterway is more effective than the rear end. In order to avoid temperature gradients due to such uneven heat distribution, which can affect the performance of the motor, we used a two-in, two-out structure, as shown in Figure 9.

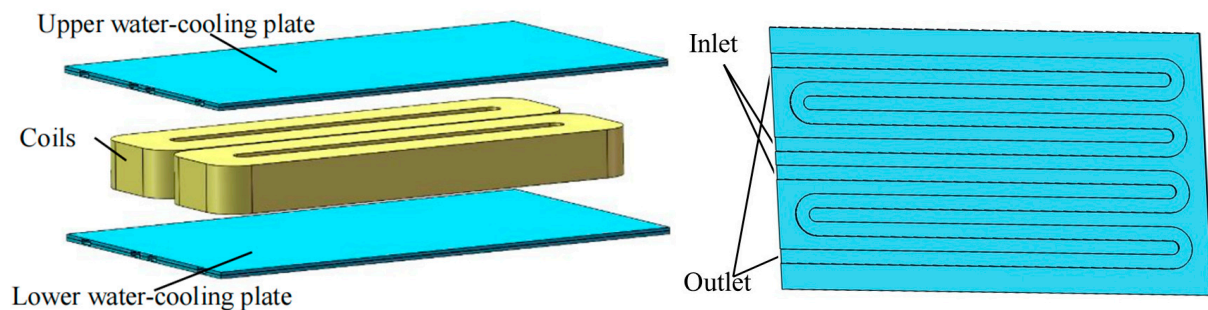


Figure 9. Cooling structure of the linear voice coil motor.

The specific dimensional parameters of the waterways in this study are shown in Table 2.

Table 2. Main parameters of the waterways.

Variable Name	Value	Unit
Water-cooling plate thickness	1.6	mm
Waterway section height	1.0	mm
Waterway section width	4.0	mm
Waterway spacing	3.8	mm

4.2. Determination of Heat Dissipation Coefficient

The single-sided, flat-type voice coil motor that was designed in this paper is a cooling structure with internal forced convection heat transfer. The relevant heat transfer parameters for the water-cooling plate were calculated using the correlation equation for

forced convection heat transfer in the tube slot. The widely used Dittus–Boelter formula can be used for such problems [9], as follows:

$$Nu = 0.023Re^{0.8}Pr^{0.3} \quad (18)$$

where Nu is Nusselt number; Re is the Reynolds number; and Pr is Prandtl number.

$$Re = \frac{ul}{\nu} \quad (19)$$

where u is the flow rate of the fluid; l is the characteristic length of the heat exchange surfaces; and ν is the kinematic viscosity of fluids.

The equivalent diameter of the watercourse was calculated as follows:

$$d_e = \frac{4A_e}{P} \quad (20)$$

where A_e is the cross-sectional area of the watercourse and P is the length of the watercourse wall in contact with the fluid.

The cooling water channel's surface heat dissipation coefficient was as follows.

$$h = \frac{\lambda_f}{d_e} Nu \quad (21)$$

where λ_f is the thermal conductivity of the cooling fluid.

Once the specific data on the cooling structure of the motor were determined, if the flow rate of the cooling medium in the cooling tube could be obtained, the cooling water channel's surface heat dissipation coefficient could also be obtained. A complete set of calculation models for the temperature field of the voice coil motor could then be constructed from this and simulated using the finite element method.

The average flow rate of the liquid in the cooling water channel was estimated using the FloXpress module in the modelling software SolidWorks, and the results are shown in Figure 10. By setting a differential pressure of 0.2 MPa between the inlet and the outlet, and by selecting water at 22 °C as the cooling medium, the average flow velocity in the longitudinal channel was approximately 4.085 m/s, and the average flow velocity in the transverse channel was approximately 1.119 m/s. According to the above formula, the water-cooled plate's heat dissipation coefficient was $3.7 \times 10^4 \text{ W}/(\text{m}^2 \cdot ^\circ\text{C})$.

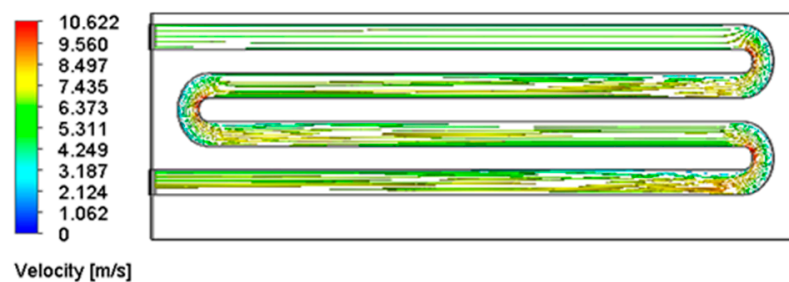


Figure 10. Graph of flow rate simulation results.

4.3. Temperature Field's Finite Element Simulation

An equivalent winding simulation model was established, based on the volume of the actual winding and on the proportional relationship between the copper and the insulation material in the winding. This is shown in Figure 11. This model captured the temperature gradient within the winding [10].

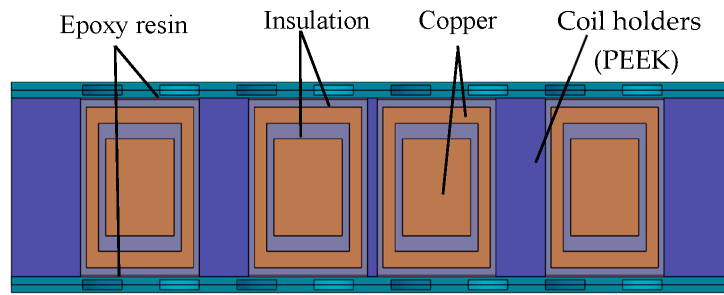


Figure 11. Equivalent winding model.

The results of the steady-state thermal analysis that was carried out in ANSYS are shown below. In this analysis, we found that a maximum temperature of 419.94 °C was obtained under natural cooling—at a current density of 13.33 A/mm²—while the maximum temperature of the motor under forced water cooling was 56.553 °C, and the simulation results are shown in Figure 12. The heat was completely trapped in the water-cooled plate and the cooling effect was obvious.

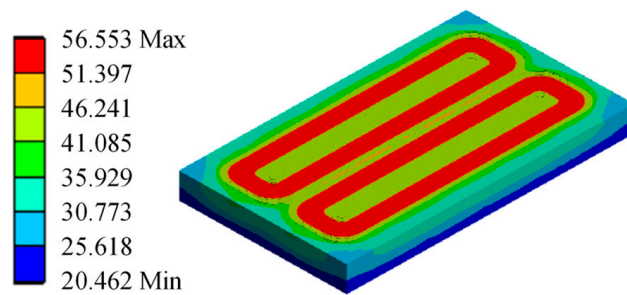


Figure 12. Forced water cooling simulation result at $J = 13.33\text{A/mm}^2$.

In order to see the cooling effect of the water-cooled plate, the relationship between the maximum temperature and current density of the motor is obtained through the simulation software, as shown in Figure 13. It can be seen that the double-layer water-cooled plate structure can greatly improve the current that the motor can withstand.

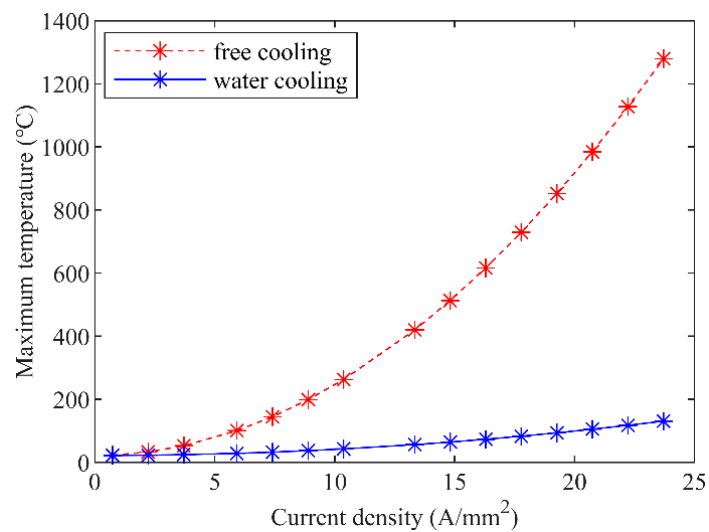


Figure 13. The relationship between maximum temperature and current density.

5. Conclusions

In this study, we designed a single-sided, flat-type, linear voice coil motor for the magnetically levitated cable table of a lithography machine. The motor used an array of Halbach permanent magnets, with a double layer of water-cooled plates, to provide x-directional thrust to the cable table. This solved the problem posed by the cables during the operation of the lithography machine. A mathematical model was established, first, by using the magnetic charge method to derive the analytical equation for the space magnetic field. After this, from the basic principle of a single-sided, flat-type voice coil motor, an analytical derivation of the horizontal thrust, generated by the motor using differential superposition, provided the basis for the establishment of the main motor parameters. The results obtained through the simulation of the motor's electromagnetic field, using finite element simulation software, were consistent with the analytical results. Using Jmag simulation software, the motor was parametrically modelled to optimize the motor's size and to obtain the optimum thrust density. A two-inlet, two-outlet serpentine waterway, with a double-layer water-cooling plate structure was designed for this motor. The effectiveness of this water-cooling structure was verified by simulating the temperature field of the motor through ANSYS Workbench.

Author Contributions: Conceptualization W.Z. and H.Z.; methodology, W.Z., J.M., and H.Z.; software, W.Z. and J.M.; writing—original draft preparation, W.Z. and S.W.; writing—review and editing, H.Z. All authors have read and agreed to the published version of the manuscript.

Funding: This research is supported by the National Natural Science Foundation of China, under grant (51877052).

Institutional Review Board Statement: Not applicable.

Informed Consent Statement: Not applicable.

Data Availability Statement: Not applicable.

Conflicts of Interest: The authors declare no conflict of interest.

References

1. Ling, Z.J.; Zhao, W.X.; Ji, J.H. Overview of high force density permanent magnet linear actuator and its key technology. *Trans. China Electrotech. Soc.* **2020**, *35*, 1022–1035.
2. Qin, W.; Fan, Y.; Xu, H.Z. A linear induction maglev motor with HTS traveling magnetic electromagnetic Halbach array. *Trans. China Electrotech. Soc.* **2018**, *33*, 5427–5434.
3. Xing, L.G.; Zhou, H.X.; Hou, S.L. Research and application of voice coil motor. *MicroMotors* **2011**, *44*, 82–87.
4. Chang, X.F.; Chen, Y.P.; Ai, W. Review of design, control and application of voice coil linear motor. *MicroMotor* **2008**, *41*, 66–69+83.
5. Zeng, J.S.; Yao, Z.Y.; Zhao, C.S. Research on nonlinear phenomena in ultrasonic motors. *China Mech. Eng.* **2006**, *17*, 1047–1050.
6. Chai, J.W.; Gui, X.G. Structural Optimization and Application Review of Voice Coil Motor. *Trans. China Electrotech. Soc.* **2021**, *36*, 1113–1125.
7. Wang, B.C.; Liu, C.; Wu, Z.W. LCL filter design and implementation for improving transient position tracking control performance of voice coil motor. *IEEE Access* **2020**, *8*, 4963–4971. [[CrossRef](#)]
8. Pan, D.H.; Li, L.Y.; Wang, M.Y. Modeling and optimization of air-core monopole linear motor based on multiphysical fields. *IEEE Trans. Ind. Electron.* **2018**, *65*, 9814–9824. [[CrossRef](#)]
9. Dai, P.J.; Xu, Y.J.; Yin, Z.B. Electromagnetic vibration power generation battery based on voice coil motor. *Electronic. Technol. Softw. Eng.* **2021**, *1*, 234–236.
10. Zhao, W.D.; Cui, S.M.; Liu, Q. Calculation and Analysis of Temperature Field of Air-Core Compensated Pulsed Alternator. *Proc. CSEE* **2011**, *31*, 95–101.

Disclaimer/Publisher's Note: The statements, opinions and data contained in all publications are solely those of the individual author(s) and contributor(s) and not of MDPI and/or the editor(s). MDPI and/or the editor(s) disclaim responsibility for any injury to people or property resulting from any ideas, methods, instructions or products referred to in the content.